Evidence of Spin-Canting, Metamagnetism, Negative Coercivity, and Slow Relaxation in a Two-dimensional Network of {Mn6} Cages

Document Version
Accepted author manuscript

[Link to publication record in Manchester Research Explorer](#)

OPEN ACCESS

Evidence of Spin-Canting, Metamagnetism, Negative Coercivity, and Slow Relaxation in a Two-dimensional Network of {Mn$_6$} Cages

Catherine Dendrinou-Samara,*[a] James P. S. Walsh,[b,c] Christopher A. Muryn,[b] David Collison,[b] Richard E. P. Winpenny,[b] and Floriana Tuna*[b]

Dedicated to the memory of Professor Olivier Kahn (1943–1999), pioneer of the molecular magnetism field.

Abstract: The synthesis, crystal structure, and magnetic studies are reported for a two-dimensional network of mixed valence {Mn$_6$} cages. The compound contains three different bridging ligands: pivalate, phenylphosphonate, and partially deprotonated triethanolamine. The result of using three bridging ligands is a complex structure involving a {Mn$^{III}_2$Mn$^{II}_4$} edge-sharing bitetrahedron that interlinks, forming a layered structure. Weak inter-cage interactions lead to a remarkably complicated magnetic behaviour, with a phase transition at 2.1 K leading to a canted anti-ferromagnetic state.

Introduction

Polynuclear manganese complexes have been the focus of extensive research in the field of molecular magnetism over the last two decades, owing to their prominent role in single-molecule magnet (SMM) research.[1] The history of these compounds can be traced back to the early nineties, when the first reports of slow magnetic relaxation in a single molecule were reported for the now well-known {Mn$_{12}$} clusters.[2,3] Although the field has since diversified to include complexes containing other metals (transition metals, lanthanoids, and mixtures thereof), manganese compounds remain popular due to the higher level of control that can be exerted over their coordination chemistry, as well as their relative stability.
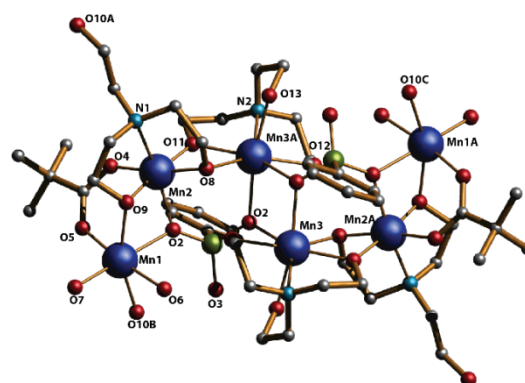
One common route to manganese clusters involves the reaction of flexible tripodal alcohols with metal carboxylate cages;[4] another uses phosphonates to displace carboxylates in order to grow larger cages.[5] In the present study, we report a single reaction that utilises both approaches at the same time. Our reasoning was that this would produce large, complex structures, and that such compounds might have unusual magnetic properties. Here, we report the crystal structure and magnetic properties of {[Mn$_6$(O$_2$C^{t}Bu)$_2$(O$_3$PPh)$_2$(Htea)$_2$(H$_2$tea)$_2$(H$_2$O)$_4$](Me$_3$COO)$_2$CH$_3$CN}$_n$ (**1**), where H$_3$tea = triethanolamine, and we document and explain an unusually complicated magnetic behaviour caused by the co-existence of several magnetic phenomena, namely spin-canting, metamagnetism, and negative coercivity. Similarly complex behaviour has been reported by others for networks of manganese,[6] and cobalt,[7] and spin-canting has been purposely targeted as an approach toward single-chain magnet (SCM) behaviour,[8] and as a method for generating weak ferromagnetism in extended frameworks.[9]

Results and Discussion

Synthesis and Structure

The starting material in the preparation of **1** was the hexanuclear mixed valence complex [Mn$_6$O$_2$(O$_2$C^{t}Bu)$_{10}$(HO$_2$C^{t}Bu)$_4$] (**2**),[10] which contains an edge-sharing bitetrahedron of manganese centres, with two Mn(III) ions in the shared edge, and four Mn(II) ions in the exterior vertices. The reaction of **2** with a mixture of PhPO$_3$H$_2$ and H$_3$tea in MeCN at room temperature gave complex **1**. The structure of **1** consists of [Mn$_6$(O$_2$C^{t}Bu)$_2$(O$_3$PPh)$_2$(Htea)$_2$(H$_2$tea)$_2$(H$_2$O)$_4$]$^{2+}$ cages linked into a two dimensional sheet within the crystallographic *bc* plane.

[a]   Prof. C. Dendrinou-Samara
        Department of Chemistry
        Aristotle University of Thessaloniki
        54124 Thessaloniki, Greece
        E-mail: samkat@chem.auth.gr

[b]   Dr. J. P. Walsh, Dr. C. A. Muryn, Prof. D. Collison,
        Prof. R. E. P. Winpenny, Dr. F. Tuna
        Department of Chemistry and Photon Science Institute
        The University of Manchester
        Oxford Road, Manchester, M13 9PL, UK
        E-mail: floriana.tuna@manchester.ac.uk

[c]   Dr J. P. S. Walsh
        Department of Chemistry
   Northwestern University
        2145 Sheridan Road, Evaston, IL 60208, USA

Figure 1. The structure of the repeat unit of **1** in the crystal. Hydrogen atoms have been omitted for clarity.

The hexanuclear repeat unit (**Figure 1**) is on a crystallographic inversion centre. There are two independent Mn(II) sites (Mn1 and Mn3) and a single Mn(III) site (Mn2); oxidation states are assigned based on BVS calculations.[10] The phosphonate ligand adopts the 4.220 bridging mode (Harris notation;[11] **Scheme 1**), with one oxygen (O2) bridging between Mn3 and its symmetry generated equivalent, while another (O1) bridges between Mn1 and Mn2. The third oxygen (O3) of the phosphonate forms a hydrogen bond to a H2tea ligand. The single independent pivalate ligand bridges Mn1 and Mn2 in a 2.11 fashion.
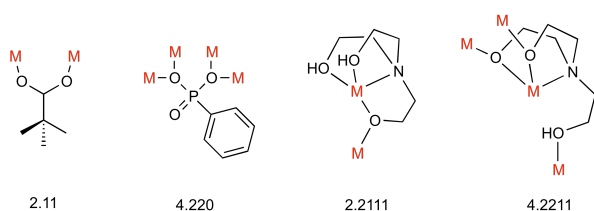
Scheme 1. The binding modes of the ligands in **1**.

There are two crystallographically independent triethanolamine ligands in the structure. One, involving N2, is assigned as an H_2tea ligand, and adopts the 2.2111 binding mode, acting as a tetradentate ligand towards Mn3 while also bridging through the μ-alkoxide to Mn2. The second, involving N1, is assigned as an Htea ligand, and adopts the 4.2211 mode, where it is tridentate towards Mn2, while O8 and O9 bridge in a μ₂-fashion to Mn3A and Mn1 respectively. One of the oxygen atoms (O10) binds to a manganese centre in a neighbouring hexanuclear unit, and is the means by which the two-dimensional polymer propagates (**Figure 2**).
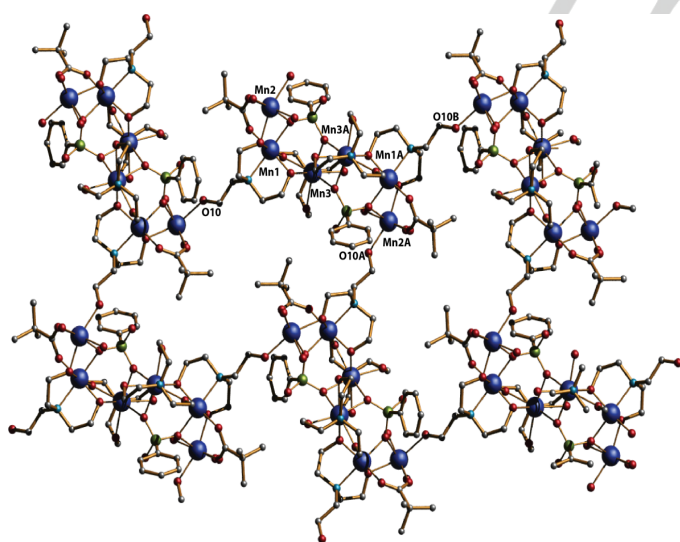
Figure 2. The two-dimensional polymer of **1** in the crystal.

The Htea undergoes hydrogen bonding to oxygen atoms from uncoordinated phosphonate groups (O10–H⋯O3(phosp.) = 2.720 Å), while both protonated arms of H_2tea are involved in two separate hydrogen bonding pathways (O13-

H13⋯O3(phosp.) = 2.577 Å, O12#–H12#⋯O8(Htea) = 2.577 Å). Additionally, the water molecule hydrogen bonds to the uncoordinated O14 atom of a pivalate molecule in the crystal lattice (O7–H7⋯O14 = 2.648 Å), while the other water molecule is hydrogen bonded to the oxygen of the symmetrical H_2tea (O6–H6⋯O12# = 2.796 Å).

The coordination environment of Mn1 is MnO_6, with bond lengths ranging from 2.17 to 2.25 Å; this is typical for Mn(II). The six oxygen donors come from a phosphonate, two Htea ligands, a carboxylate oxygen, and two water molecules. Mn2 is six-coordinate, with a $MnNO_5$ coordination sphere, and a Jahn-Teller elongation typical of Mn(III) centres. The Htea ligand provides the N-donor (N1) that occupies one apical position (Mn2–N1 = 2.301(5) Å), while the other apical position is occupied by O1 from a phosphonate (Mn2–O1 = 2.124(4) Å).

The two Jahn-Teller axes of Mn2 and Mn2A are parallel to each other. The N1–Mn2–O1 angle is slightly bent, reaching 161.63(0)°, as has also been observed in other Mn(III) complexes.[12] The equatorial positions around Mn2 are occupied by O8 and O9 from the Htea, O4 from a pivalate, and O11 from the H_2tea ligand. The bond lengths within the equatorial plane fall within the range 1.88–2.01 Å, which is significantly shorter than the apical bonds. Mn3 is seven coordinate, with a $MnNO_6$ coordination sphere.

The singly deprotonated triethanolamine H_2tea provides the atoms O11, O12, O13, and N2, while the other coordination sites are completed by atoms from Htea (O8 and the symmetry equivalent of O10), and from a phosphonate group (O2); bond lengths to Mn3 fall within the range 2.20–2.46 Å, supporting its assignment as Mn(II). The shortest distances between manganese centres are Mn1⋯Mn2 = 3.171(2), Mn2⋯Mn3 = 3.246(2), and Mn3⋯Mn3 = 3.520(7) Å.

The two-dimensional network is formed via links between O10 and Mn1 in the repeat units, and creates a structure that contains four hexanuclear units arranged about a parallelogram. The long edge of the parallelogram contains all six manganese centres from one hexanuclear unit, while the short edge is formed by Mn1 and Mn2 from another unit (**Figure 2**). This arrangement leads to two different orientations of the {Mn_6} repeat units, with a split angle between their Jahn-Teller axes of 9.6°, and also leads to the formation of cavities within the structure, each containing two pivalic acid and two MeCN molecules. The closest Mn⋯Mn distance between the {Mn_6} units within the layers is 7.745(3) Å, while the nearest interlayer Mn⋯Mn distance is 7.903 (5) Å.

Magnetic Properties

The magnetic susceptibility of compound **1** was measured in the 1.8–300 K temperature range in applied magnetic fields ranging from 0.1 to 10 kG. Plots of $\chi_M T$ *vs.* T for **1** (χ_M is the molar paramagnetic susceptibility per {Mn_6} unit) at 0.1 and 1 kG are shown in **Figure 3**. At 300 K, $\chi_M T$ is 22.9 cm³ K mol⁻¹, a value that is close to the spin-only value of 23.5 cm³ K mol⁻¹ (assuming g = 2) expected for a {Mn_6} unit comprising two high-spin Mn(III) and four high-spin Mn(II) ions.
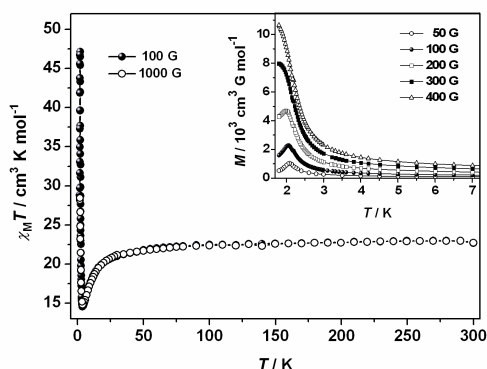
Figure 3. Plots of $\chi_M T$ vs. T for compound **1** at 100 and 1000 G. Inset: field-cooled magnetisation at various fields.

Upon cooling, $\chi_M T$ decreases, first gradually and then more rapidly below 50 K to reach a rounded minimum of *ca.* 14.7 cm³ K mol⁻¹ at 4.5 K (corresponding to an $S = 5$ total spin). Upon further cooling it increases rapidly to a very high, strongly field-dependent and sharp maximum of 47.14 cm³ K mol⁻¹ at 2.07 K (under a 100 G applied magnetic field), which is characteristic of a long-range magnetic ordering, before finally decreasing again to reach 28.80 cm³ K mol⁻¹ at 1.8 K. The magnetic susceptibility data in the temperature range 20–300 K can be well fitted with the Curie-Weiss law, $\chi = C/(T\text{-}\theta)$, giving C = 23.15 cm³ K mol⁻¹ and θ = −3.32 K, for the Curie and Weiss constants, respectively. The small size and negative sign of θ is indicative of weak antiferromagnetism in **1**. However, the sharp upturn of $\chi_M T$ below 4.5 K suggests the occurrence of intra-layer ferromagnetic-like correlations due to spin canting[13] of the antiferromagnetically coupled {Mn$_6$} entities.
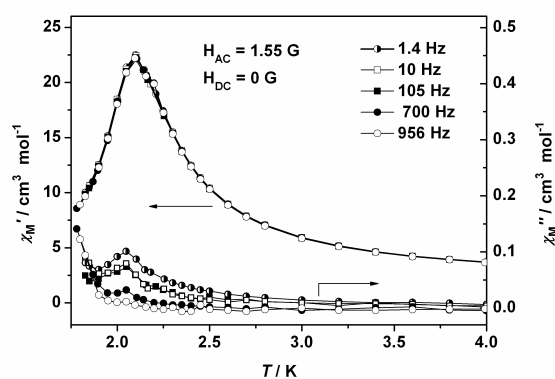
The decrease in $\chi_M T$ below T_{max} = 2.07 K is most likely due to saturation effects and/or inter-layer antiferromagnetic interactions.[14] This is verified by comparing the field-cooled (FC) and zero-field-cooled (ZFC) magnetisations of **1** at low temperatures. In a small external field of 50 G, both magnetisation curves show a maximum at 2.1 K (**Figure 4**), indicative of antiferromagnetic ordering.[15] Below 2.1 K, however, the FC magnetization curve diverges from that measured in a ZFC regime, indicating the presence of a small remnant magnetization, whose size increases upon cooling.
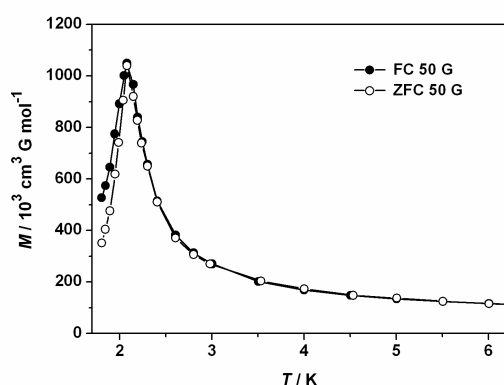
These features indicate that compound **1** has a partly canted antiferromagnetic structure below *ca.* 2.1 K. This is further confirmed by variable-temperature *ac* susceptibility measurements at zero *dc* field, which show a frequency-independent maximum in both the *in-phase* (χ_M') and *out-of-phase* (χ_M'') components of the ac susceptibility, located at 2.1 and 2.06 K respectively (**Figure 5**). The latter—which is the signature of a magnetised state[14]—is two orders of magnitude smaller in intensity than the maximum in $\chi_M'(T)$, indicating weak ferromagnetism induced by spin canting. This behaviour is typical for canted antiferromagnets,[16] and evidences the appearance, below a critical temperature, of a small spontaneous magnetisation in a predominantly antiferromagnetic phase, caused by the failure of spins in different sublattices to arrange strictly antiparallel to one another. This situation gives rise to uncompensated magnetic moments that become correlated in a ferromagnetic-like fashion and develop into long range magnetic ordering below the critical temperature. The canting of spins is consistent with the structural features of compound **1**, *i.e.* the presence of a two dimensional network (**Figure 2**) composed of anisotropic {Mn$_6$} hexametallic units with two different orientations of the Jahn-Teller axes (each of which corresponds to the local easy-axis of the {Mn$_6$} magnetisation). A series of temperature scans in various fields (the inset of Figure 3) reveals a strong dependence of the low-temperature phase upon the strength of the applied magnetic field, H. For example, the field-cooled magnetization curves recorded with magnetic fields $H \leq 200$ G present a $M(T)$ maximum at *ca.* 2.1 K, indicating the onset of three-dimentional antiferromagnetic ordering between spin-canted layers. In contrast, the magnetisation curves recorded in magnetic fields of 300 G or higher show no maximum, but tend
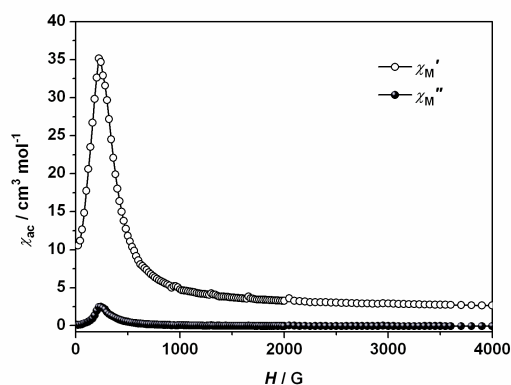

Figure 4. The temperature dependence of the field-cooled (FC) (filled circles) and zero-field cooled (ZFC) (open circles) magnetization of **1** measured at 50 G applied field.

Figure 5. The temperature dependence of the real, χ', and imaginary, χ'', components of the *ac* susceptibility of **1** measured in a zero *dc* field and 1.55 G *ac* field oscillating at the indicated frequencies.

Figure 6. The in-phase and out-of-phase susceptibilities versus *dc* field for **1,** recorded at 1.8 K with an *ac* field of 1.55 G oscillating at a frequency of 10 Hz.

to saturate at lower temperatures, thus indicating that a magnetic field between 200 and 300 G is sufficient to overcome these weak interactions. Compound **1** therefore presents a field-induced transition from an antiferromagnetic to a ferromagnetic-like state.

This behaviour is indicative of a metamagnet built of spin-canted antiferromagnetic layers.[17] The metamagnetic transition reveals itself as a sharp peak at the critical field of 240 G in both the in-phase and out-of-phase *ac* magnetic susceptibilities of **1**, measured at 1.8 K and 10 Hz, as a function of the *dc* field (**Figure 6**). The small value of the critical field can be accounted by considering the small interactions (through space) between the spins of the $\{Mn_6\}$ subunits, which are separated by 7.7–7.9 Å.

The spin canting and metamagnetic behaviours of **1** were also confirmed by field-dependent isothermal magnetisation measurements. Plots of *M vs. H* at temperatures above and below the transition temperature are shown in the inset of Figure 7. At 4 K there is a steady increase in *M* with field without reaching saturation up to a field of 70 kG. At temperatures below the transition temperature, however, the *M vs. H* curves display the sigmoidal shape typical of metamagnets.[17,18] The 1.8 K isotherm shows very little magnetization until *ca.* 150 G—as is typical for an antiferromagnet—after which the magnetisation increases rapidly with increasing field to reach 3.1 $N_{\mu B}$ at *ca.* 800 G, indicating a spin-flipping transition from an antiferromagnetic arrangement to a weak ferromagnetic arrangement. The magnetization then increases more slowly, approaching a value of 22.5 $N_{\mu B}$ at 70 kG without showing true saturation.

The plots of *M vs. H/T* at different temperatures do not superpose on a single master curve, suggesting the presence of a significant anisotropy in **1**, and/or the population of low-lying excited states, which is expected to occur in Mn(II)/Mn(III) complexes.[19] Indeed, the *M-H* isotherms at 1.8 and 2 K display an inflection point at about 20 kG and at a little above 10 $N_{\mu B}$, indicating a spin-change within the $\{Mn_6\}$ subunits. The metamagnetic transition occurs at the critical field of *ca.* 240 G (*i.e.* the field at which a maximum d*M*/d*H* value is reached) and

at 1.8 K, in full agreement with the *ac* susceptibility (**Figure 6**) and field-cooled magnetisation data (the inset of **Figure 3**). We ascribe this transition to the field-induced reversal of the canted spins of the $\{Mn_6\}$ subunits that comprise the two-dimensional lattice in **1** from an antiparallel to a parallel configuration. Extrapolation of the high field linear part of the magnetisation curve to zero field gives a magnetisation value of 3.2 $N_{\mu B}$. Assuming this is the uncompensated magnetisation per $\{Mn_6\}$ unit, the spin-canting angle can then be calculated[20] as $\alpha = \tan^{-1}(M_r/M_s) = 8.1°$ (where $M_s = 22.5$ $N_{\mu B}$), which is in good agreement with the structural features of **1** and the angle of 9.6° between the $\{Mn_6\}$ Jahn-Teller axes.

Interestingly, the low-field magnetisation curve at 1.8 K displays an uncommon butterfly-shaped inverted hysteresis (**Figure 7b**), with a coercive field of 22 G and a negative remnant magnetization of *ca.* −0.034 $N_{\mu B}$. The metamagnetic behaviour is evident from the shape of the central part of the hysteresis loop, however, the existence of a magnetisation inverted hysteresis in a molecular magnet is rare. This uncommon behaviour contrasts with that of conventional ferromagnets, in which *M* turns positive even though the applied field maintains negative, and *vice versa,* and has only been observed in some rare cases of inorganic layered and alloy systems,[21] as well as in two molecular magnets belonging to the family [M(Cp*)₂][Ni(α-
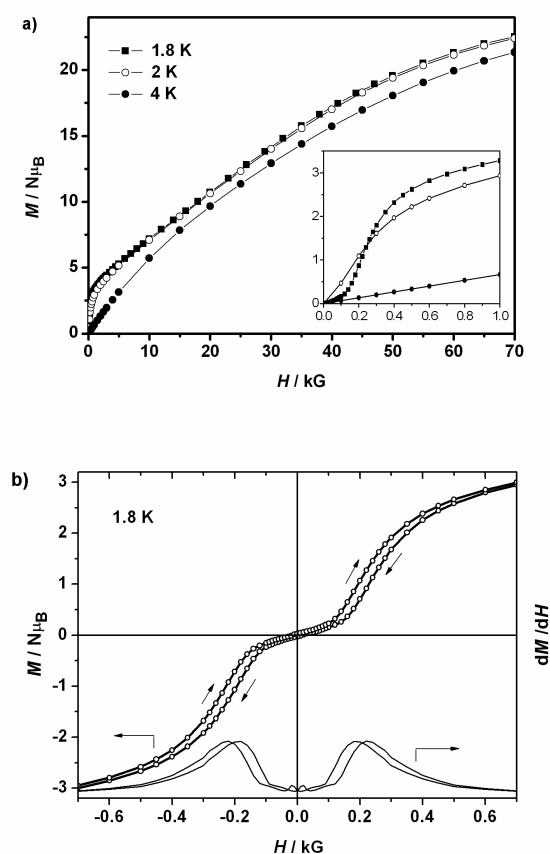
Figure 7. a) Field dependence of the magnetization for **1**. The inset shows the low-field parts of the magnetization curves at 1.8, 2 and 4 K . b) Hysteresis loop (open circles) and dM/dH (solid line) of **1** observed at 1.8 K.

tpdt)$_2$], where M = Fe, Mn, and α-tpdt = 2,3-thiophenedithiolate.[22]

The negative coercivity in these compounds was associated with their thin-film or layered structures and attributed to the competition between sublattice magnetisation rotation induced by a spin-flip transition and the trapping effect caused by the uniaxial magnetic anisotropy. The origin of the inverted hysteresis in **1** is not fully understood, but it seems reasonable to assume that this effect is related to the layered structure of **1**, and to the field-induced reversal of the spins of the highly anisotropic {Mn$_6$} components from an antiferromagnetic to a ferromagnetic configuration.

Close inspection of **Figure 5** reveals a second increase of $\chi_M''(T)$ at zero *dc* field with decreasing temperature below *ca.*1.95 K. To examine this behaviour further, we performed *ac* susceptibility measurements under applied *dc* fields ranging from 0 to 1000 G, using an *ac* field of 1.55 G oscillating at 956 Hz (**Figure 8**). Upon varying the *dc* field from 0 to 200 G, the peak in χ_M' (indicative of antiferromagnetic ordering) increases in magnitude, and the maximum shifts to lower temperature; the maximum value is at 1.87 K under a 200 G external field (inset of **Figure 8a**). At higher fields, the peak in χ_M'' loses intensity and does not appear

to shift in temperature. A second peak starts to appear at higher temperature, and by 600 G this second peak is slightly more intense than the first, with a maximum at 2.25 K (the inset of **Figure 8b**). At 1000 G only the second peak is seen, and the maximum has shifted to around 2.43 K. The out-of-phase susceptibility, χ_M'', increases at low temperature, with the most dramatic increase under an external field of 200 G (**Figure 8a**). At external fields of 600 G and above there is a broad weak peak in χ_M''; this peak is found around 0.1 K lower in temperature than the higher temperature peak observed for χ_M' at the same external fields (**Figure 8b**).

In a 200 G *dc* field (Figure 9a), both $\chi_M'(T)$ and $\chi_M''(T)$ exhibit strong frequency-dependence, indicative of slow relaxation of the magnetisation. Moreover, the *ac* susceptibility at a 600 G *dc* field indicates the occurrence of two different magnetic transitions (**Figure 9a**). The $\chi_M'(T)$ curve shows a frequency-independent peak at 2.26 K, and another peak at *ca.* 1.9 K, which is strongly frequency-dependent. Similarly, $\chi_M''(T)$ displays a weak and broad peak at 2.18 K, which is frequency independent, and a second increase below 2 K, which is strongly frequency-dependent.
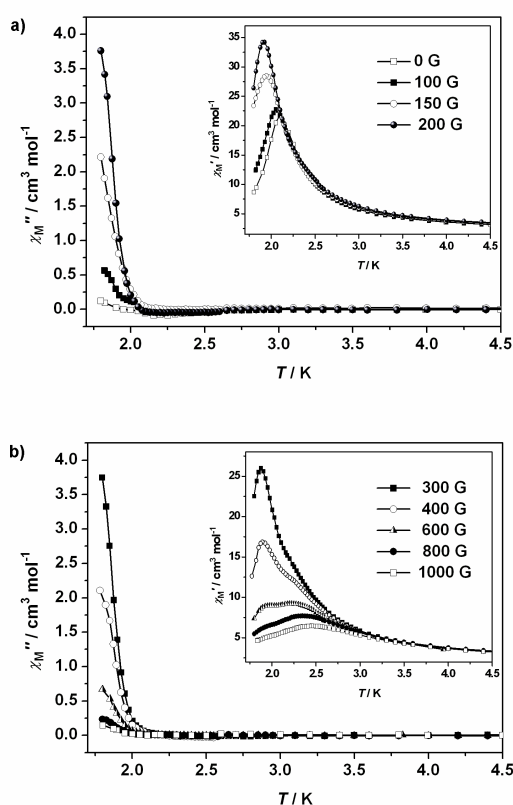
Figure 8. The temperature dependence of the real, χ_M', and imaginary, χ_M'', components of the *ac* susceptibility of **1** measured in an *ac* field of 1.55 G oscillating at 956 Hz, and in applied *dc* fields of a) 0, 100, 150 and 200 G, and b) 300, 400, 600, 800 and 1000G.
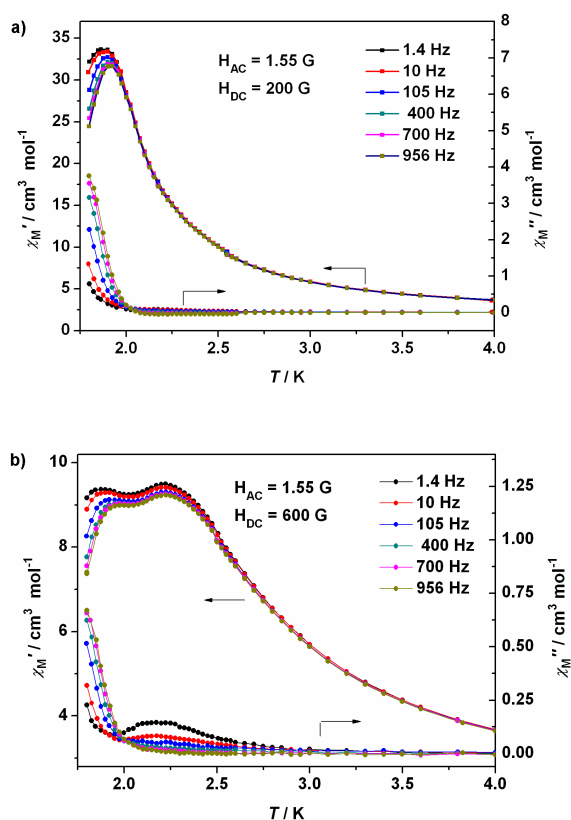
Figure 9. The temperature dependence of the real, χ_M', and imaginary, χ_M'', components of the *ac* susceptibility of **1** measured in applied *dc* fields of a) 200 G, and b) 600 G, under 1.55 G *ac* field oscillating at the indicated frequencies.
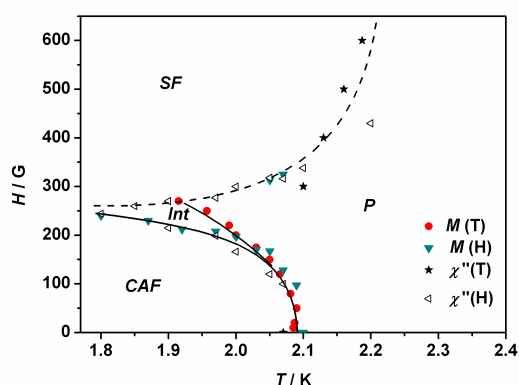
Figure 10. The phase diagram of compound **1**.

Figure 10 shows the H_c vs. T phase diagram of **1**, deduced from ac susceptibility and dc magnetisation measurements as a function of temperature and magnetic field. A canted antiferromagnetic (CAF) to paramagnetic (P) phase transition is observed at ca. 2.1 K, and at very small magnetic fields. Because of the canting between the spins of the {Mn$_6$} entities in **1**, a pure antiferromagnetic three-dimensional ordering is not achieved, and thus this material behaves as a very weak ferromagnet with spontaneous magnetisation below ca. 2.06 K (i.e. the temperature at which the imaginary component of the ac susceptibility at zero dc field displays a frequency-independent peak). This magnetic ordering can be overcome by an external magnetic field that induces a transition to a spin-flop (SF) ordered phase, or to a paramagnetic phase. The resulting field-induced ferromagnetic region appears to be separated from the paramagnetic phase by an unclear boundary (dashed line in Figure 10, data points extracted from broad peaks in the ac susceptibility), and thus cannot be accurately assigned to a proper phase transition. There is also an intermediate phase between the CAF and SF regions, whose origin is unknown at this moment. However, a similar intermediate region was observed in a recently reported Fe/Ni molecular magnet[20] that also exhibits an uncommon magnetization inverted hysteresis loop, as observed in **1**.

Conclusions

The use of triethanolamine and phosphonate ligands has provided a useful route to an interesting two-dimensional network of covalently linked {Mn(II)$_4$Mn(III)$_2$} entities with two different orientations of their Jahn-Teller axes. This compound shows a quite unusual and complex magnetic behaviour, displaying simultaneously weak ferromagnetism below T_c, spin canting, slow relaxation, metamagnetic behaviour, and an unusual reversed hysteresis loop. Such complicated behaviour is unprecedented in molecule-based systems, and originates from both the strong anisotropy of the hexametallic clusters that

form the two-dimensional structure of **1**, and the dipolar interactions between them.

The complicated magnetic behaviour is due largely to the complexity of the structure. There is clear evidence of canting of molecular moments, however canting cannot occur within individual {Mn$_6$} units because the Jahn-Teller axes of the two Mn(III) ions in such units are parallel. Within layers, however, there are two types of {Mn$_6$} units whose Jahn-Teller axes make an angle of ca 9.6° to each other, and this is the source of the canting. The intra-layer connection between {Mn$_6$} clusters involves an ethanolamine arm, and the shortest Mn⋯Mn separation is 7.7 Å. There is no inter-layer bonding, and the minimum separation is 7.9 Å; therefore, inter-cluster interactions must be very weak. When the external field is increased, the tendency of the spins to align parallel with the field overrides these weak inter-cluster antiferromagnetic interactions. Because of the canting, a pure antiferromagnetic phase cannot be achieved, and **1** shows a very weak ferromagnetism below the critical temperature.

Experimental Section

Preparation of Compounds

All reagents, metal salts, and ligands were used as obtained from Sigma Aldrich. [Mn$_6$O$_2$(O$_2$C^{t}Bu)$_{10}$(HO$_2$C^{t}Bu)$_4$] (**2**) was prepared following a literature method.[7]

{[Mn$_6$(O$_2$C^{t}Bu)$_2$(O$_3$PPh)$_2$(Htea)$_2$(H$_2$tea)$_2$(H$_2$O)$_4$](Me$_3$COO)$_2$CH$_3$CN}$_n$ (1)
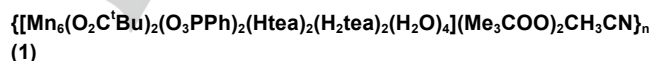
A brown solution of **2** (0.25 g, 0.14 mmol) in MeCN (10 mL) was treated with a suspension of PhPO$_3$H$_2$ (0.017 g, 0.11 mmol) and triethanolamine (0.14 mL, 0.93 mmol). The resulting solution was stirred for 4 h and then filtered. Crystals suitable for X-ray diffraction studies grew from the cognac-brown filtrate after 5 days. Yield: 40%. Elemental analysis calcd. (%) for C$_{58}$H$_{111}$Mn$_6$N$_5$O$_{30}$P$_2$: C 39.85, H 6.39, N 4.00; found: C 39.12, H 6.57, N 3.89.

Structure Determination

Data were collected on an Oxford Xcalibur CCD diffractometer (Mo-Kα, λ = 0.71069 Å). The selected crystal was mounted on the tip of a glass pin using Paratone-N oil and placed in the cold flow (100 K) produced by an Oxford Cryocooling device.[23] Complete hemispheres of data were collected using ω-scans (0.3°, 30 seconds per frame). Integrated intensities were obtained using the program SAINT+,[24] and were corrected for absorption using the program SADABS.[25] Structure solution and refinement was performed with the SHELX package.[25] The structure was solved by direct methods and completed by iterative cycles of ΔF syntheses and full-matrix least-squares refinement against F^2. Crystal data are given in Table 1. CCDC reference number 1029261 contains the supplementary crystallographic data for this paper. These data can be obtained free of charge from the Cambridge Crystallographic Data Centre via www.ccdc.cam.ac.uk/data_request/cif.

Physical Measurements

Magnetic measurements were performed on polycrystalline samples restrained in eicosane using a Quantum Design MPMS-XL

SQUID magnetometer equipped with a 7 T magnet. Data were corrected for the diamagnetism of the compound using Pascal constants, and for the diamagnetic contributions of the sample holder and eicosane by measurement. Direct current (*dc*) measurements were collected at temperatures over the range 1.8–300 K, and applied magnetic fields between −70 and 70 kG. Alternating current (*ac*) measurements were recorded using a 1.55 G magnetic field oscillating at frequencies between 1 and 1000 Hz, and under various *dc* magnetic fields ranging from 0 to 6 kG.

Table 1. Crystallographic Details for **1**

Compound	1
formula	$C_{58}H_{111}Mn_6N_5O_{30}P_2$
fw[1]	1750.1
cryst syst	monoclinic
space group	$C2/c$
a, Å	23.437(1)
b, Å	18.197(1)
c, Å	19.897(1)
β, deg	106.231(5)
V, Å^3	8147.5(9)
T, K	150(2)
Z	4
ρ_{calcd}, g cm^{-3}	1.427
λ, Å / μ, mm^{-1}	0.71073 / 1.019
no. of reflns collected / $2\Theta_{max}$, deg	40274 / 25
no. of reflns unique / $I >2\sigma(I)$	7068 / 4454
no. of params / restraints	494 / 2
R$_1$ / goodness of fit	0.0692 / 1.032
wR_2 ($I >2\sigma(I)$)	0.1617
residual density, e Å^{-3}	0.85 / -0.40

Acknowledgements

[1]   a) G. Aromi and E. K. Brechin, *Struct. Bonding* **2006**, *122*, 1; b) J. Ferrando-Soria, J. Vallejo, M. Castellano, J. Martinez-Lillo, E. Pardo, J. Cano, I. Castro, F. Lloret, R. Ruiz-Garcia, M. Julve, *Coord. Chem. Rev.* **2017**, *339*, 17; c) V. A. Milway, F. Tuna, A. R. Farrell, L. E. Sharp, S. Parsons, M. Murrie, *Angew. Chem. Int. Ed.* **2013**, *52*, 1949-1952.

[2]   a) A. Caneschi, D. Gatteschi, J. Laugier, P. Rey, R. Sessoli, C. Zanchini, *J. Am. Chem. Soc.* **1991**, *113*, 5873; b) R. Sessoli, D. Gatteschi, A. Caneschi, M. A. Novak, *Nature* **1993**, *353*, 141.

[3]   a) R. Sessoli, H.-L. Tsai, A. R. Schake, S. Wang, J. B. Vincent, K. Folting, D. Gatteschi, G. Christou, D. N. Hendrickson, *J. Am. Chem. Soc.* **1993**, *115*, 1804; b) C. Benelli, D. Gatteschi, Introduction to molecular magnetism: from transition metals to lanthanides, Wiley VCH, **2015,** 195.

[4]   a) C. J. Milios, M. Manoli, G. Rajamaran, A. Mishra, L. E. Budd, F. White, S. Parsons, W. Wernsdorfer, G. Christou and E. K. Brenchin, *Inorg. Chem.* **2006**, *45*, 6782; b) M. Murugesu, W. Wernsdorfer, K. A. Abboud, G. Christou, *Angew. Chem.* **2005**, *117*, 914.

[5]   C. Boskovic, M. Pink, J. C. Huffman, D. N. Hendrickson, G. Christou, *J. Am. Chem. Soc.* **2001**, *123*, 9914.

[6]   a) O. Roubeau and R. Clerac, *Eur. J. Inorg. Chem.* **2008**, 4325; b) X.-Y. Wang, L. Wang, Z.M. Wang, G. Su, S. Gao, *Chem. Mater.* **2005**, *17*, 6369.

[7]   a) N. Marino, T. F. Mastropietro, D. Armentano, G. De Munno, R. P. Doyle, F. Lloret, M. Julve, *Dalton Trans.* **2008**, 5152; b) A. V. Palii, O. S. Reu, S. M. Ostrovsky, S. I. Klokishner, B. S. Tsukerblat, Z.-M. Sun, J.-G. Mao, A. V. Prosvirin, H.-H. Zhao, K. R. Dunbar, *J. Am. Chem. Soc.* **2008**, *130*, 14729.

[8]   a) K. Bernot, J. Luzon, R. Sessoli, A. Vindigni, J. Thion, S. Richter, D. Leclercq, J. Larionova, A. van der Lee, *J. Am. Chem. Soc.* **2008**, *130*, 1619; b) W.-X. Zhang, R. Ishikawa, B. Breedlove, M. Yamashita, *RSC Adv.* **2013**, *3*, 3772.

[9]   D.-F. Weng, Z.-M. Wang, S. Gao, *Chem. Soc. Rev.* **2011**, *40*, 3157.

[10]   A. G. Blockman, J. C. Huffman, E. B. Lobkovsky, G. Christou, *Polyhedron* **1992**, *11*, 251.

[11]   Harris notation describes the binding mode as [X.Y1Y2Y3…Yn], where X is the overall number of metals bound by the whole ligand, and each value of Y refers to the number of metal atoms attached to the different donor atoms. *See*: R. A. Coxall, S. G. Harris, D. K. Henderson, S. Parsons, P. A. Tasker, R. E. P. Winpenny, *J. Chem. Soc. Dalton Trans*. **2000**, 2349.

[12]   H. Miyasaka, K. Nakata, L. Lecren, C. Coulon, Y. Nakazawa, T. Fujisaki, K. Sugiura, M. Yamashita, R. Clérac, *J. Am. Chem. Soc.*, **2006**, *128*, 3770.

[13]   O. Kahn, Molecular Magnetism , VCH Publishers, New York, **1993**, 322.

[14]   M.-H. Zeng, W.-X. Zhang, X.- Z. Sun, X.-M. Chen, *Angew. Chem. Int. Ed.* **2005**, *44*, 3079.

[15]   a) B.-P. Yang, A. V. Prosvirin, Y.-Q. Guo, J.-G. Mao, *Inorg. Chem.* **2008**, *47*, 1453; b) Y.-Z. Zheng, W. Xue, M.-L. Tong, X.-M. Chen, F. Grandjean, J. Long, *Inorg. Chem.* **2008**, *47*, 4077.

[16]   a) R. L. Carlin, *Magnetochemistry*, Springer-Verlag, Heidelberg, **1986**; b) E.-Q. Go, P.-P. Liu, Y.-Q. Wang, Q. Yue, Q.-L. Wang, *Chem. Eur. J.* **2009**, *15*, 1217.

[17]   E.-Q. Gao, Z.-M. Wang and C.-H. Yan, *Chem. Commun.* **2003**, 1748.

[18]   a) C. L. M. Pereira, E. F. Pedroso, H. O. Stumpf, M. A. Novak, L. Richard, R. Ruiz-Garcia, E. Riviere and Y. Journaux, *Angew. Chem. Int. Ed.* **2004**, *43*, 956; b) K. Chandra Mondal, G. E. Kostakis, Y. Lan, C. E. Anson, A. K. Powell, *Inorg. Chem.* **2009**, *48*, 9205; (c) E. Coronado, J. R. Galán-Mascarós, C. J. Gómez-García, A. Murcia-Martínez, *Chem. Eur. J.* **2006**, *12*, 3484.

[19]   S. K. Langley, K. J. Berry, B. Moubaraki, K. S. Murray, *Dalton Trans.* **2009**, 973.

[20]   C. Bellito, F. Federici, M. Colapietro, G. Portalone and D. Caschera, *Inorg. Chem.* **2002**, *41*, 709.

[21]   a) S. Ohkoshi, T. Hozumi, K. Hashimoto, *Phys. Rev. B.* **2001**, *64*, 132404; b) M. J. O'Shea, A. L. Al-Shariff, *J. Appl. Phys.* **1994**, *75*, 6673.

[22]   D. Belo, L. C. J. Pereira, M. Almeida, C. Rovira, J. Veciana, V. Gama, *Dalton Trans.* **2009**, 4176.

[23]   J. Cosier, A. M. Glazer, *J. Appl. Crystallogr.* **1986**, *19*, 105.

[24]   *SHELX-PC Package.* Bruker Analytical X-ray Systems: Madison, WI, **1998**.

[25]   W. Liu, H. H. Thorp, *Inorg. Chem.* **1993**, *32*, 4102.

Entry for the Table of Contents (Please choose one layout)

Layout 1:

FULL PAPER

A 2D network of covalently linked {Mn$_2^{III}$Mn$_4^{II}$} entities with two different orientations of their Jahn-Teller axes and complex magnetic behaviour, displaying simultaneously weak ferromagnetism, spin canting, slow magnetic relaxation, metamagnetic behaviour and an unusual reversed hysteresis.
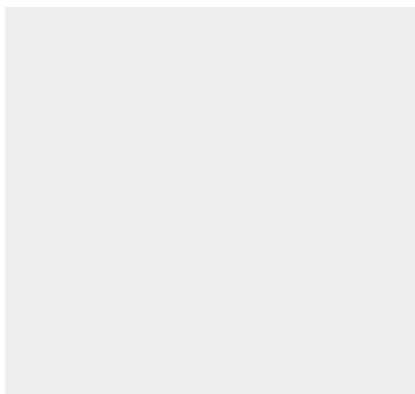
Key Topic: Spin canting and Metamagnetic behaviour

Author(s), Corresponding Author(s)*

Page No. – Page No.

Title

*spin canting and metamagnetic behaviour